Open Ceramics 9 (2022) 100211

Contents lists available at ScienceDirect

Open Ceramics

journal homepage: www.sciencedirect.com/journal/open-ceramics

Top-down material design of multi-phase ceramics

S. Pirkelmann, F. Raether, G. Seifert *

Fraunhofer-Zentrum für Hochtemperatur-Leichtbau HTL, Gottlieb-Keim-Str. 62, 95448, Bayreuth, Germany

ARTICLE INFO

Keywords:
Microstructure-property simulation
Material design
Multi-phase ceramics
ICME
Machine learning

ABSTRACT

A methodology for the top-down design of ceramic materials composed of two or more phases has been developed. It is demonstrated on the example of the well-known alumina/zirconia (AZ) material system. Core of the method is an automated simulation chain based on representative volume elements for generating a database of microstructure-property relations. The database emanating from this simulation chain was used to train machine learning models for enabling fast predictions of material microstructure according to preset material properties. A gradient boosting algorithm provided reliable and fast calculations for the exemplary chosen thermal and mechanical properties of the AZ material system. This enables reverse identification of selected microstructural parameters needed to obtain a specific value of a material property of interest, or briefly: top-down ceramic material design.

1. Introduction

In recent years, materials research and development has been advanced considerably by the implementation of digital methods on various length scales and for many steps along the value chain. This statement holds, in particular, for metals and alloys, where the concept of integrated computational materials engineering (ICME) meanwhile has found its way in the industrial application [1,2]. In this field, many software tools were developed and are being offered now for simulation of phenomena from crystal growth on atomic scales to high-cycle fatigue of large components under typical loads during application [3]. Automatized coupling of modeling and experiments on different length scales yields, e.g., correlations between microstructural parameters and application behavior, which can be used to identify the production conditions for optimum performance of the parts to be produced [4]. Machine learning algorithms like neural networks provide a powerful toolbox to find these downward correlations in the sense of top-down design [5–7]. In spite of the scientific progress in this field, however, mostly only individual elements of ICME are utilized for practical development projects due to the still existing challenges in computation and model verification.

Digitalization of material development in the field of ceramics has not yet reached a comparably advanced level. Ceramic materials require different approaches for processing and property simulation than metals, precluding in many cases the direct use of models established for metallic materials. Besides vastly different preparation procedures, a crucial difference is the brittleness of ceramics. While in metals plastic deformation can relax local thermal stresses from the production process, the stresses in the microstructure after cooling down a material from sinter temperature to room temperature are usually a critical issue for the strength of the material. Researchers worldwide have meanwhile successfully modeled almost all relevant steps of ceramic manufacturing individually by various simulation methods (e.g., spray drying [8], powder compaction [9]; drying [10], debinding [11] and sintering [12, 13] of ceramic components) and can predict material properties based on microstructure models [14,15]. However, a comprehensive approach linking all these techniques together in the sense of an integrated computational ceramics engineering (ICCE) is missing up to date.

As was pointed out in the review on ICME by Panchal et al. [16], top-down material design must explicitly include the material structure in a multiscale approach, which can be linked to the processing conditions forming these structures as well as to the application properties resulting from structural details of the material. In that sense, simplified material concepts like the well-known Voigt-Reuss-Hill average [17] or Hashin-Shtrikman bounds [18,19] are not sufficient to enable inverse material design. Also concepts regarding the microstructure more explicitly like Ondracek's model [20] are usually not suited for describing composites with high contrast between the phases, thin layers at grain interfaces or percolation phenomena. In general, advanced questions like the structure-dependent distribution of thermal

* Corresponding author.
E-mail addresses: simon.pirkelmann@isc.fraunhofer.de (S. Pirkelmann), friedrich.raether@isc.fraunhofer.de (F. Raether), gerhard.seifert@isc.fraunhofer.de (G. Seifert).

https://doi.org/10.1016/j.oceram.2021.100211
Received 3 December 2021; Accepted 20 December 2021
Available online 22 December 2021
2666-5395/© 2021 The Authors. Published by Elsevier Ltd on behalf of European Ceramic Society. This is an open access article under the CC BY-NC-ND license (http://creativecommons.org/licenses/by-nc-nd/4.0/).

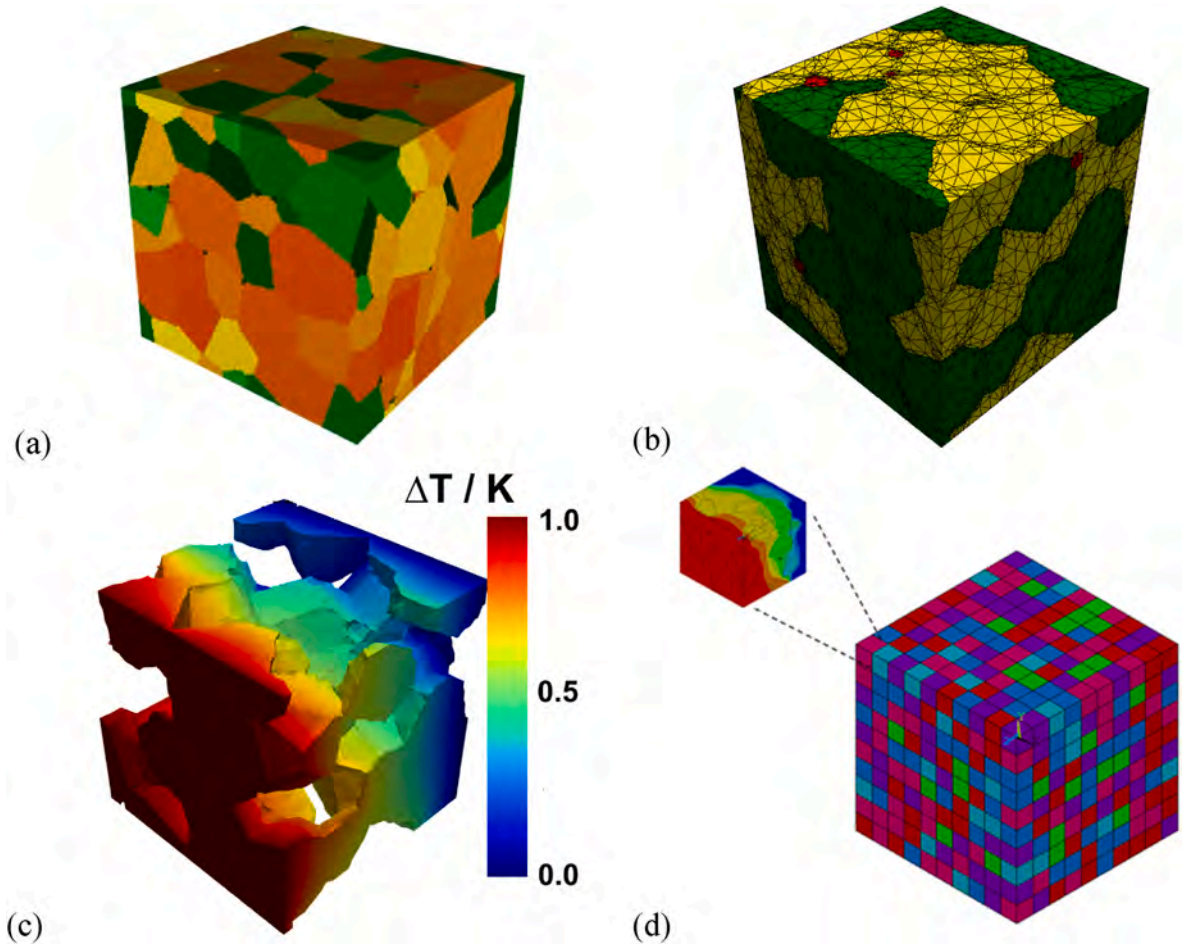

Fig. 1. (a) example for an RVE composed of Voronoi polyhedra for a two-phase ceramic composite; (b) meshed RVE used as input for FE simulations; (c) FE result for temperature distribution in a single phase of the composite yielding thermal conductivity; (d) illustration of homogenization technique by a large-scale grid composed of small RVE with stochastic orientation.

stresses cannot be answered by any of these models but require explicit structure-related simulations.

In this work, we describe the development and first application of an automated simulation chain for studying microstructure-property relations of ceramic materials, with the potential to provide the above-described functionality. The components of this simulation methodology, which is based on representative volume elements (RVE) have been developed and validated against experimental results on mechanical, thermal and electrical properties for many different ceramic composites in the last years [21–23]. The simulation chain is used to generate a database of mechanical and thermal material properties for the example of the alumina/zirconia material system (including pores as third phase). The use of machine learning tools for the reverse problem, i.e., identification of microstructural parameters required to achieve a preset material property is demonstrated.

2. Materials and methods

2.1. Key elements for simulation of material properties

Our concept for predicting the material properties of ceramics composed of more than one phase relies on the broadly accepted approach of representative volume elements (RVE) with periodic boundary conditions. Material properties of the composite are calculated by help of finite element analysis in dependence of the microstructural characteristics, using material properties of the pure phases as input. The components of the simulation chain have been described in detail in previous publications [21–23]; a brief overview is given in the following.

According to a recent review by Bargmann et al. [24], the generation of 3D RVE can be classified into three categories: (i) reconstruction from experimental characterization of real samples, (ii) methods intending to simulate the physical processes of microstructure formation and (iii) purely geometrical constructions with focus on mimicking the morphology. An In-house software (called GeoVal) for RVE generation combines elements of categories (ii) and (iii) to allow for a material design on the one hand, which on the other hand accounts for the ceramic material-specific physical processes such as forming or sintering in a realistic way. In that sense, microstructure generation always starts out geometrically with introducing spheres at random positions within the RVE. Spheres of several different phases with individually different average sizes and size distributions can be introduced. These spheres are then redistributed according to hard sphere repulsion in order to simulate the particle rearrangement during forming processes like spray drying or slip casting. Next, the spheres are converted into the required particle shapes for each phase, for instance into prisms, platonic solids or Voronoi-polyhedra. Irregularity of particle shapes, as they are introduced, e.g., by milling, are considered by cutting particles at random planes. Particle sizes are then adapted to match a preset volume fraction of the respective phase by growth or shrinkage operations followed by further rearrangement including reorientation to minimize particle overlap.

At this point the geometrical objects (typically 50 to 250) are converted into a voxel structure, enabling voxel-based stochastic procedures

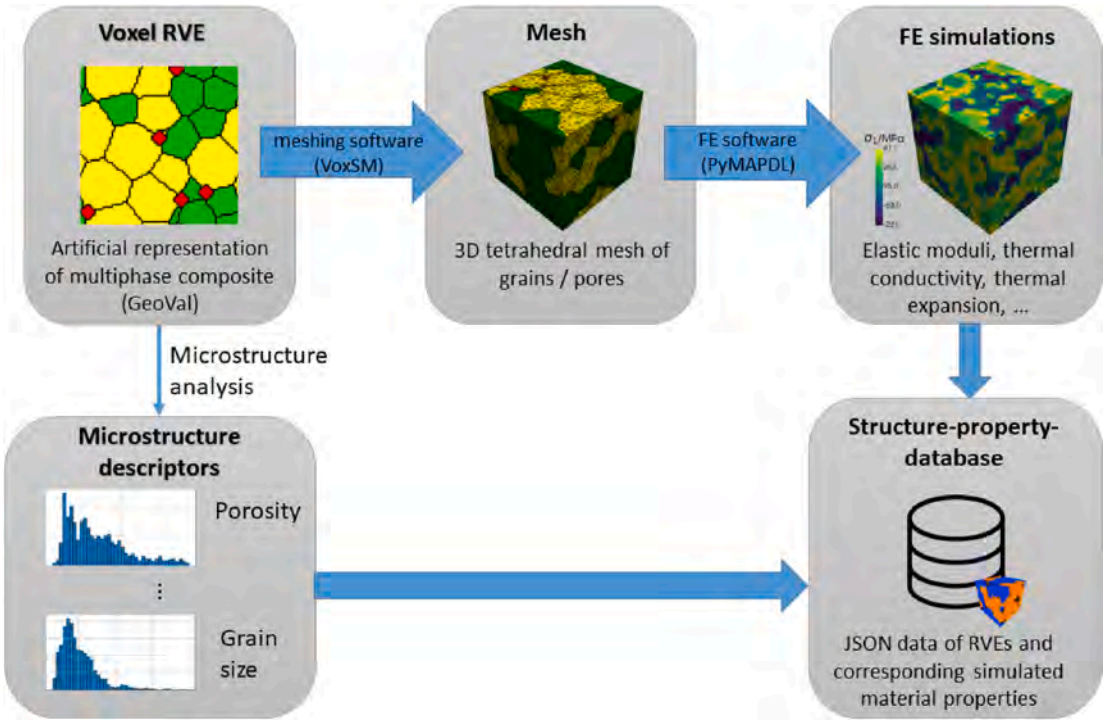

Fig. 2. Framework for automated microstructure-property simulations.

Table 1
Summary of average computation times (in seconds) of each step of the simulation chain for RVEs of different resolution. The data shown represents the mean and standard deviations of the measured times for several hundreds of structures.

RVE dimension (voxels)	Voxel structure generation	RVE meshing	Simulation and Postprocessing (PyMAPDL)		
			Elasticity	Thermal conductivity	Thermal expansion
32	28 ± 25	608 ± 114	227 ± 30	37 ± 6	67 ± 35
64	204 ± 128	3623 ± 834	260 ± 30	51 ± 5	71 ± 7

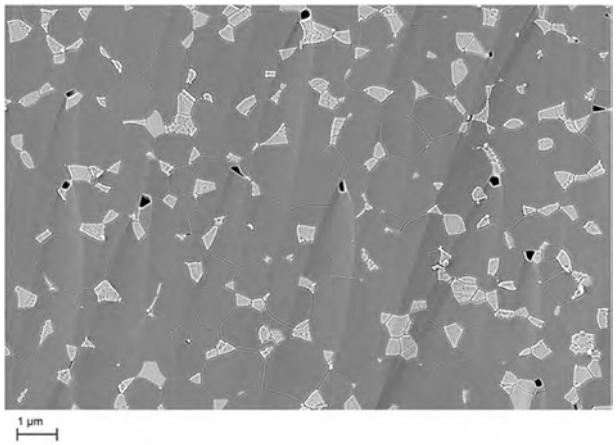

Fig. 3. SEM image showing the microstructure of a ZA ceramic; dark gray: alumina; light gray: zirconia; black: pores.

for generating for example pores at corners or edges. Also, interphases at interfaces as they can result from liquid phase sintering can be introduced. Typical RVE comprise 32^3, 64^3 or 128^3 voxels, depending on the number of particles and type of microstructure: while smooth structures like Voronoi-polyhedra can often be represented with sufficient precision already with 32^3 voxels, materials composed of particles with high aspect ratio, splintery shapes or simply broad size distribution require larger RVE. The software allows for quantitative measures of structural properties of the voxel structure as they are described in Ref. [25]. E.g., chord length analyses of the microstructure generated in the RVE are used for quantitative comparison with real, experimentally determined microstructures.

Fig. 1(a) shows an example of an RVE composed of 120 particles (Voronoi-polyhedra) in voxel representation (128^3). Different particle sizes of the initial particles were considered using the radical plane method [26]. Phase 1 (plotted in shades of green) comprises 32%, phase 2 (plotted in yellow to orange colors) about 67% of the RVE volume; the remainder of about 1% was attributed to small pores at particle corners.

The second step of the simulation chain is the creation of a suitable mesh for finite element simulation, which represents the shapes and volumes of all particles and pores correctly but avoids the artifacts and high computational load to be expected from a mesh generated directly on the voxel structure. For that purpose, another in-house algorithm (VoxSM) converts the voxel mesh in several smoothing and simplification steps into a triangular surface mesh keeping the original information about particles, phases and their volume fraction [21]. The number of nodes is reduced from about 300,000 (in case of a 64^3 RVE) to roughly 20,000 to 40,000 during mesh conversion (cf. Fig. 1(b)). This surface mesh is finally used to generate a volume mesh for the FE software ANSYS, with the option to include explicitly a thin layer of elements at grain boundaries, which is required for instance for simulations of electrical properties [21].

Next, the volume mesh is used for calculating macroscopic material properties of the composite for the specific RVE microstructure by FE analyses. By applying loads in different directions like a small amount of mechanical strain, electrical potential or temperature differences in the FE model (illustrated in Fig. 1(c)), the stiffness matrix as well as

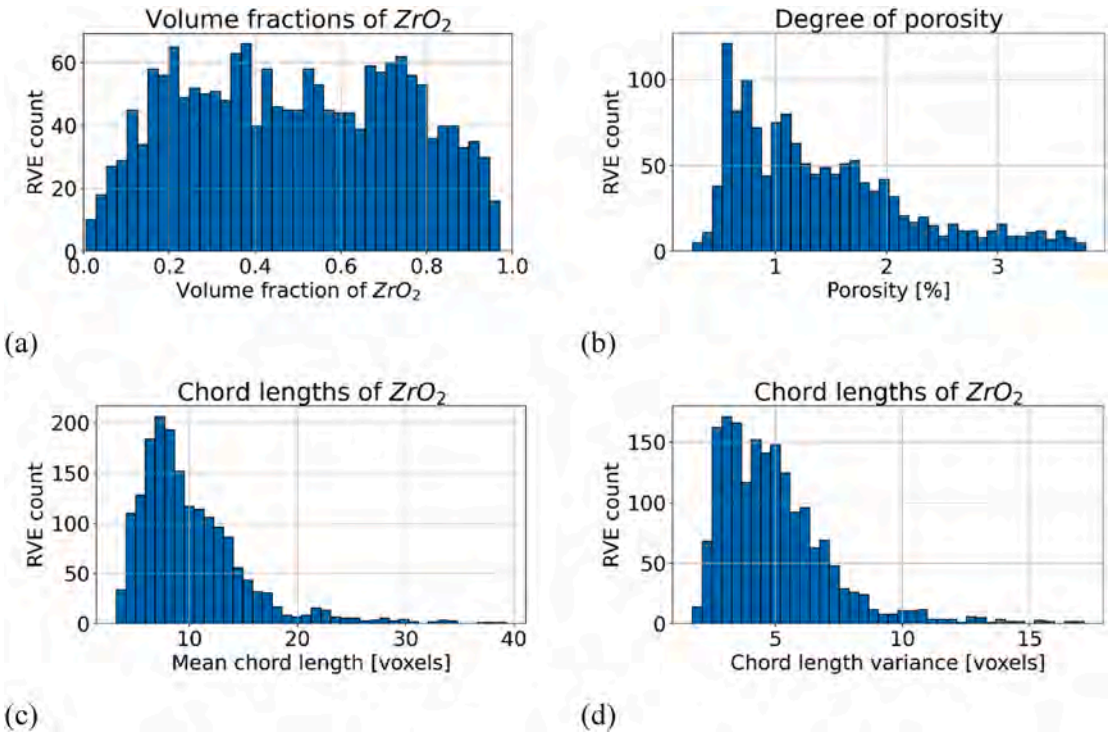

Fig. 4. Distributions of various microstructure parameters for the structures in the generated RVE database.

electrical impedance and thermal conductivity tensors of the RVE are obtained. Coefficients of thermal expansion can also be derived easily from evaluating the RVE size change after a small temperature change. A further evaluation of this latter FE result yields the distribution of thermal stresses in the microstructure as they occur during the cooling down after sintering for most ceramic composites. These stress distributions can be interpreted as a relative measure of intrinsic failure probability of a material [14].

Due to the periodic boundary conditions, this FE simulation provides in simple cases already a fair approach to the macroscopic properties. In case of isotropic materials, as is the case for many sintered ceramics, remaining anisotropies caused by the limited RVE size are removed by a final homogenization step. For that, we generate a 'super-cell' composed of, e.g., 20^3 voxels which are assigned the property component values obtained for the RVE along its principal axes, but with a stochastic rotation of the tensors obtained in the first step. The principle is illustrated in Fig. 1(d), where the different orientations of the individual RVE are indicated by different colors. By applying the same FE loads as described for the small RVEs, homogenized macroscopic properties emerge.

Finally, to account for the variety of local microstructures which are generated by the stochastic algorithms in GeoVal, usually several initial RVEs with identical composition and microstructure parameters are created and evaluated by the described simulation chain. Previously, results were averaged and validated by comparison with experimental data from composites with identical chord length distribution. The very good agreement of the material properties predicted with this methodology has already been demonstrated for various multi-phase ceramic systems [21–23]. Instead of averaging results directly, we use them now creating a broad database to train machine learning algorithms.

2.2. Automation of simulation chain

To enable structure and mesh generation of a large number of RVEs, an application programming interface (API) has been added allowing external control of the in-house programs through the Python programming language. Using this interface, numerous RVE structures with a variety of microstructure parameters can be generated and meshed automatically using scripts. Similarly, the generation of the volume meshes, the FE simulations and the homogenization step have also been fully automated. The PyMAPDL interface library [27] is used, which gives access to the MAPDL process from within Python. Starting from the surface mesh of an RVE, a Python program takes control of preparing and loading the simulation mesh into Ansys, setting up the necessary boundary conditions and running the simulations, as well as the post-processing. The results of each simulation are stored in the widely used JSON format. This also includes the associated input parameters (e.g., descriptive parameters of the RVE structure, material data of the individual phases and options for the simulation). This way, the entire process can be traced and repeated at any time. A schematic overview of the individual steps of the automatic simulation chain and the tools used in the process is given in Fig. 2.

The computational effort for a single run of the automatic simulation chain depends primarily on the resolution and complexity of the voxel structure. Table 1 gives an impression of the processing times on a machine with 12 core Intel Xenon E5-2680 processor with 250 GB of memory. Most of the computational time is incurred in converting the voxel structures into the triangular surface mesh, while the time to generate the initial voxel structures is less significant. However, both voxel structure and mesh generation can run in parallel for multiple structures, allowing the processing of up to several hundred structures per day.[1]

Thus, for many materials, the relevant parameter range of microstructure descriptors can be covered in a manageable time (typically 1–2 weeks for several hundreds to a few thousand different RVEs). The resulting material properties are used to construct a comprehensive database of structure-property relationships. In the following section it will be described, how this data set can be used to train machine learning models with the aim of developing a predictive model for the properties of a material based on a given microstructure.

[1] In principle, the FE simulation of the structures can also be parallelized if enough licenses for the ANSYS software are available.

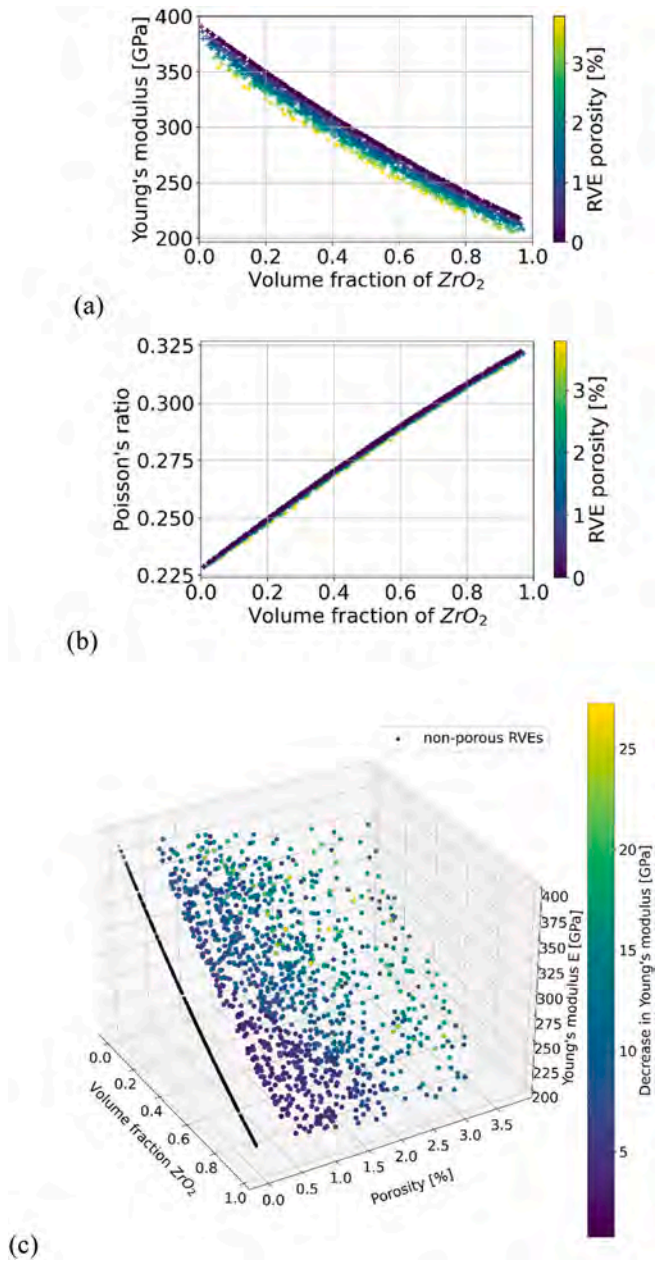

Fig. 5. Simulated elastic material properties for RVEs in the database. Each data point corresponds to a single structure. (a) Young's modulus for varying volume fractions of ZrO_2. (b) Poisson's ratio for varying volume fractions of ZrO_2. (c) Decrease of Young's modulus with increasing porosity of the structures compared to non-porous composites with varying volume fractions of the ZrO_2 phase (shown in black).

2.3. Parameter identification for top-down material design

Final goal of the work described in this paper is a top-down identification of suitable microstructural parameters for a specified material property. Searching for such a reverse correlation from simulation result to structure descriptors is a classical regression problem. Today, a variety of machine learning (ML) models is available to solve such problems (see, e.g. Ref. [28], for a comprehensive overview). For the purposes of this work, multiple regression methods implemented in the freely available Python library scikit-learn [29] were investigated by training them to predict material properties for new, unseen structures using the data pairs from a structure-property database.

In the following, the general procedure for training a regression model is briefly described. First, it is necessary to decide which feature variables should be used as input parameters in the model and which outputs the model should provide.

The definition of the features can be done manually based on prior knowledge or can be supported by a correlation analysis to identify important and less important features. In our case, the feature variables were defined manually, focusing on easily quantifiable microstructure descriptors such as the volume fraction of each phase, the mean grain sizes and their variances. Ideally, these can be measured on real samples with little effort, facilitating the validation of the final model. Some other conceivable input parameters of the model, such as the operating temperature or the material data of the individual phases and their uncertainties, were considered constant for this work. The output parameters of the model are given by material properties of interest available in the structure-property database. To keep the current paper concise, we focus on the following mechanical and thermal properties implemented in the automated simulation toolchain:

- Linear elasticity: Young's modulus, Poisson's ratio, shear modulus, bulk modulus
- Thermal conductivity
- Coefficient of thermal expansion
- Thermal stresses in each phase

With inputs and outputs of the model defined, the training can commence. To avoid overfitting, the total set of structure-property pairs is first divided into two disjoint subsets, a training set and a test set. Next, a specific type of model is selected for training and hyperparameters of the model are fixed. The training is performed, taking into account only the training set portion of the data. After training, the score of the resulting model is evaluated on the test set. If the model's performance is not satisfactory, hyperparameters of the model can be varied and different models can be tried. During the process of finding the best model and its optimal parameters, a cross-validation strategy is applied to prevent overfitting to the test set.

The major advantage of the presented approach over the alternative route via direct FE simulation is the drastic reduction in computational time for property prediction. In contrast to simulation-based property prediction, the prediction of the ML models is practically instantaneous. This makes it possible to embed them into an optimization procedure and to quickly examine the parameter space for compositions respectively microstructures with desired properties, i.e. for answering the reverse question.

2.4. Brief overview of alumina/zirconia binary material system

In order to demonstrate the capabilities of the above-described automated simulation chain and ML models, the well-known binary alumina-zirconia (AZ) material system has been chosen. AZ (or ZA) ceramics can be prepared at any composition between pure alumina and pure zirconia, and the validity of our concept of microstructure-property simulation on the basis of Voronoi-polyhedra has been proven previously for this material system [21]. As to the considerable differences of mechanical, thermal and electrical properties of alumina and zirconia, this material systems provides an instructive example for the effects of microstructural parameters such as volume fraction, relative particle size or porosity on macroscopic material properties.

Fig. 3 shows a SEM image of the microstructure of a ZA ceramic with volume fractions of 85.2% alumina (dark gray grains), 14.2% zirconia (light gray grains) and a porosity of 0.6%. The mean chord lengths of the grains have been measured to be (0.75 ± 0.2) μm (alumina) and (0.3 ± 0.08) μm (zirconia). The pores are located at the particle corners.

3. Results and discussion

The microstructure-property simulation chain was applied to the AZ

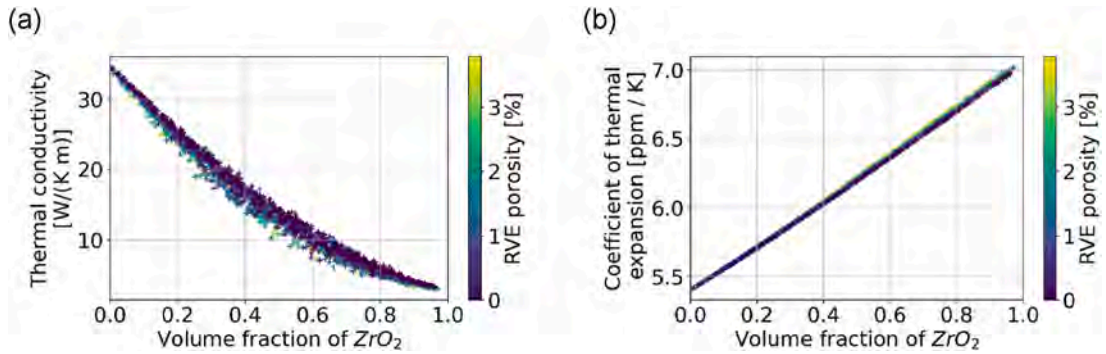

Fig. 6. Simulated material properties of the structures in the RVE database for (a) thermal conductivity and (b) coefficient of thermal expansion.

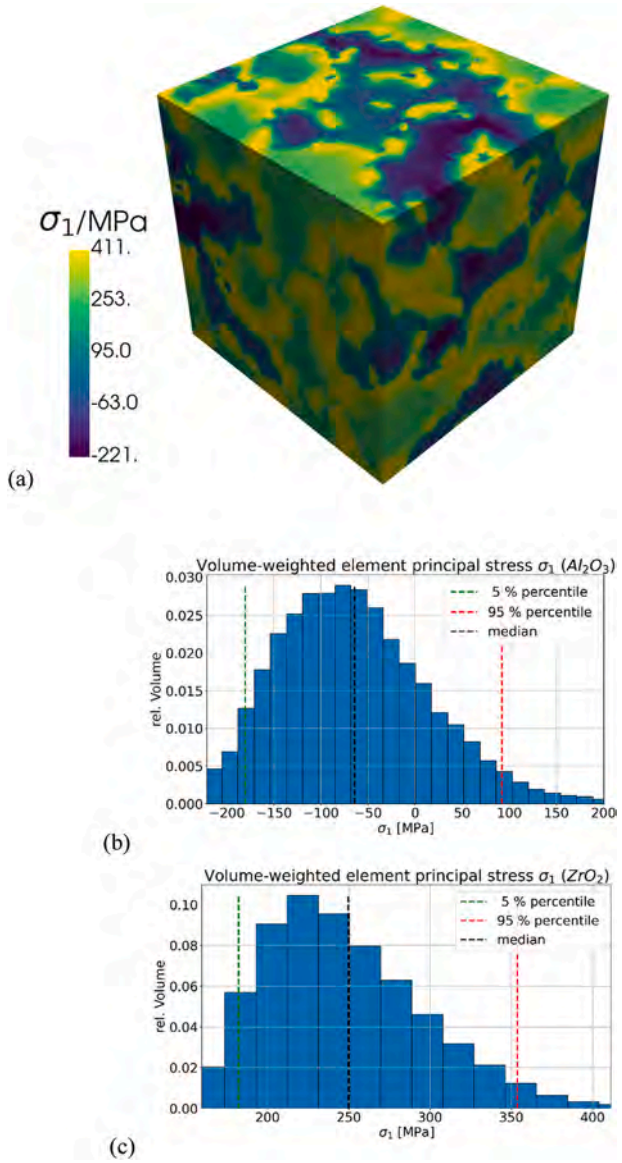

Fig. 7. (a) Visualization of principal stresses in the RVE for a cooling by 1000 K. (b) and (c): histograms and percentiles of volume-weighted distributions of principal stresses in the alumina phase (b) and zirconia phase (c).

material system. A script was used to generate artificial RVEs mimicking the microstructure of real ceramics, as shown in the SEM image in Fig. 3. Depending on the input parameters of the script, structures with different volume fractions of the two phases and chord length distributions of their particles (e.g., monodisperse, polydisperse, multimodal) are generated. In order to cover the full range of volume fractions and a reasonably broad range of particle sizes and size distributions, an algorithm randomly selects new parameters for each RVE as follows:

1. Pick a number n in [50, 100] representing the total number of particles
2. Pick a target volume fraction v1 in [0,1]
3. Randomly split the n particles into two sets n1 and n2
4. Define a radius (r1 and r2) for each set n1 and n2 so that the total sum of the sphere volumes corresponds to RVE volume

Then, as described in chapter 2.1, a redistribution of the spheres using hard sphere repulsion followed by conversion to the prefinal structure is done by a Voronoi tessellation. As last step, various degrees of porosity are added to the RVE by voxel-based operations, the pores being represented as a third phase typically located at the corners where three or more particles meet.

In this way, a database with more than 1500 RVEs of different resolutions (32^3 and 64^3 Voxels) was generated. The higher resolution was used in particular for the evaluation of stress distribution within an RVE due to thermal expansion. Porosity was either excluded or varied in the range of 0.25%–3.5%. For each generated RVE the following structural parameters were monitored:

- volume fraction of each phase
- porosity
- average chord length for grains of each phase
- variance of chord length for grains of each phase

Table 2
Prediction accuracy of the trained ML models for each material property. We list the mean and standard deviation of the score on the test set as achieved by different models trained using a 5-fold cross-validation. In addition, the root mean squared error (RMSE) on the test set is reported.

Material property	Score of training with 5-fold cross-validation			
	Mean	Standard deviation	RMSE	Unit
Young's modulus	0.999	$3.2{\cdot}10^{-4}$	1.1	GPa
Poisson's ratio	1.000	$8.5{\cdot}10^{-5}$	$3.9{\cdot}10^{-4}$	
Thermal conductivity	0.998	$4.7{\cdot}10^{-4}$	$4.1{\cdot}10^{-1}$	W/(K m)
Coefficient of thermal expansion	1.000	$5.5{\cdot}10^{-5}$	$4.8{\cdot}10^{-3}$	ppm/K
95-percentile of principal thermal stress in ZrO_2 phase	0.997	$7.9{\cdot}10^{-3}$	$7.3{\cdot}10^{-3}$	MPa

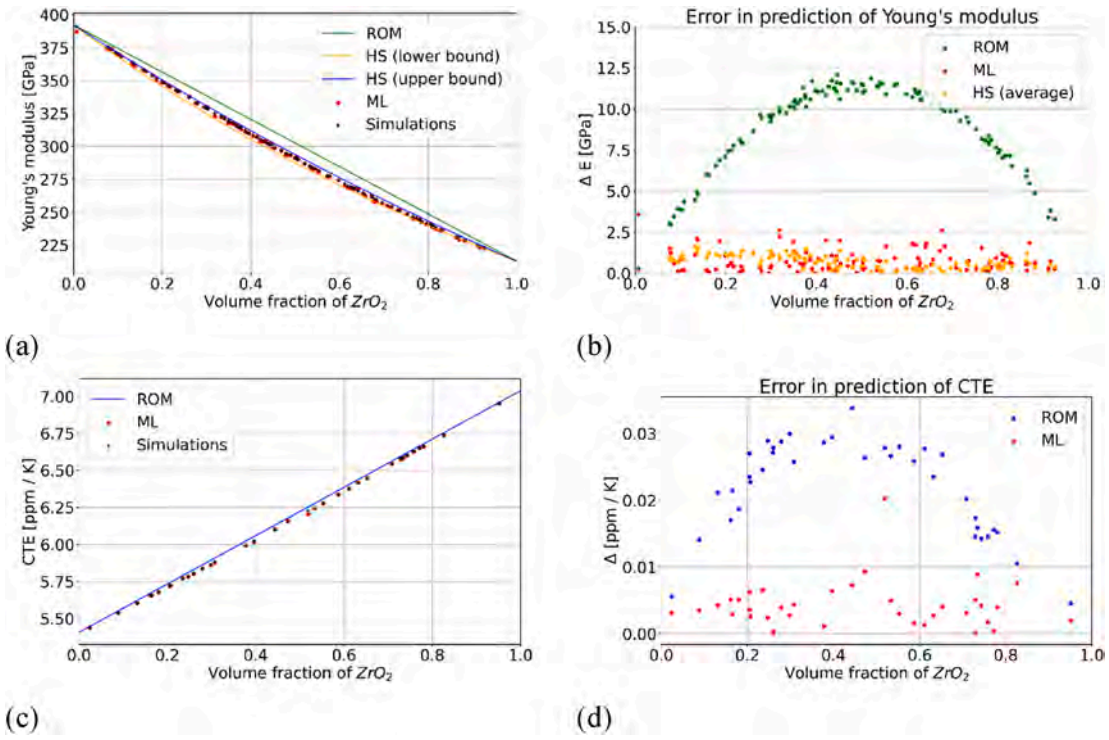

Fig. 8. Comparison of the prediction accuracy of the ROM and HS vs. the trained ML model for RVEs without porosity in the test set. (a) shows the predicted Young's modulus and the error of the prediction in (b). (c) shows the predictions for the CTE with the error plotted in (d).

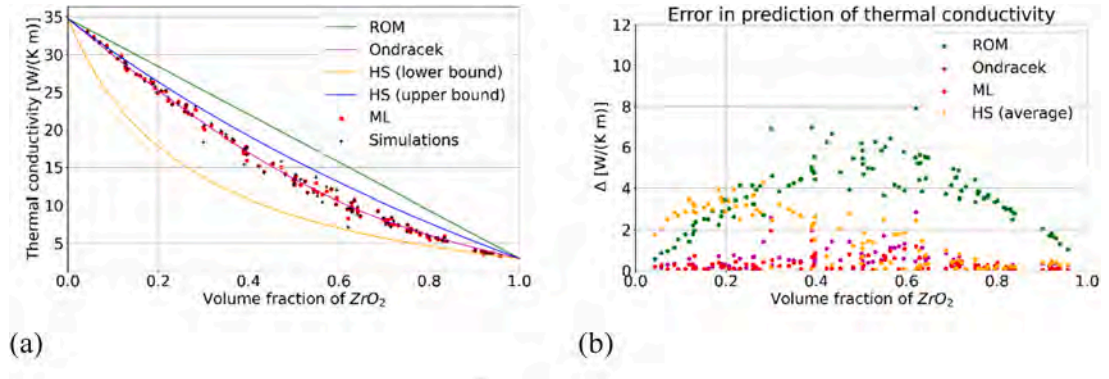

Fig. 9. Predictions (a) and error (b) for the thermal conductivity of RVEs in the test set according to different models. The root mean square errors are given by $RMSE_{ML} = 0.44$, $RMSE_{Ondracek} = 0.70$, $RMSE_{ROM} = 4.15$, $RMSE_{HS} = 1.98$.

Fig. 4 showcases the distribution of some of these statistical properties in the RVE database.

For each RVE, FE simulations were performed to calculate the elastic moduli, thermal conductivity and thermal expansion. The total time required for RVE generation, meshing and simulation was about 320 h on a 12 core Intel Xenon E5-2680 machine with 250 GB of memory. For the simulations, material data of the constituent phases at 25 °C from a commercial material database[2] were used.

Fig. 5 depicts the predicted Young's modulus and Poisson's ratio, both for RVEs with and without pores. Without porosity, the elastic parameters of the RVE are fully determined by the ratio of volume fractions of zirconia vs. alumina. It is well known that pores have significant influence on the elastic properties of ceramics, a fact that is confirmed and quantified by the simulations (cf. Fig. 5(c)).

Likewise, simulations for the thermal conductivity and the coefficient of thermal expansion (CTE) were carried out. The results of these simulations for the RVEs in the database are displayed in Fig. 6. In contrast to the simulations of elasticity, the porosity of the structure is not monotonously correlated to the thermal conductivity; in particular, porosity has almost no effect on the thermal expansion of the material. This is consistent with experimental results (see, e.g., the work of Hirata on porous sintered alumina [30]).

Another aspect of simulating thermal expansion is much more interesting: due to the different thermal expansion coefficients of the individual phases of the composite, any temperature change will lead to a distribution of thermal stresses within the microstructure. This is of practical relevance, because during cooling down to room temperature, any sintered ceramics will undergo a period of pure elastic deformation over a temperature interval of typically several hundred K. As a result, the room temperature ceramics has often quite high thermal stresses in

[2] More precisely, the data for alpha-Al_2O_3 (unique ID 2648) and 97 ZrO_2, 3 Y_2O_3 (mol%) (unique ID 666) from MPDB v9.17 (2021) by JAHM Software, Inc. was used.

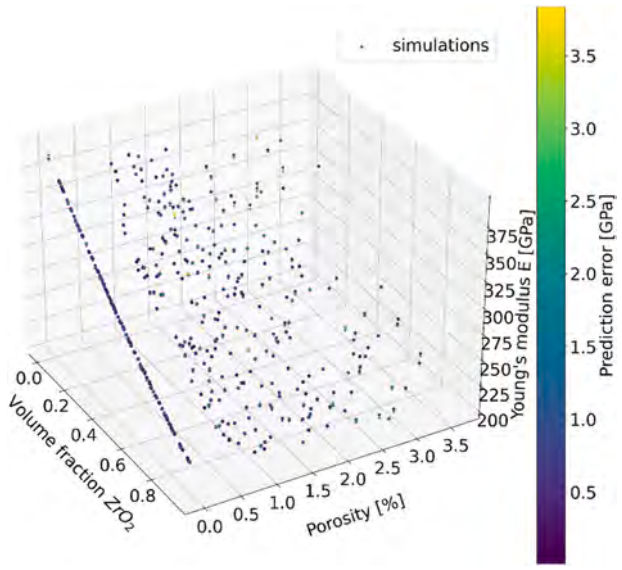

Fig. 10. Predictions of the ML model for Young's modulus of RVEs with and without porosity in the test set. The color represents the error of the model's predictions with a maximum deviation of 3.83 GPa and a RMSE of 1.14 GPa. (For interpretation of the references to color in this figure legend, the reader is referred to the Web version of this article.)

the microstructure. Since particularly tensile stresses may cause crack initiation, it can be an important design criterion for structural ceramics - or whenever the strength of a material is crucial - to minimize the amount of local tensile stresses in the microstructure.

The thermal expansion simulations provide this kind of information on the stresses in the microstructure after a temperature change. Fig. 7 (a) shows an example of the principal stresses of a ZA-composite with about 64% ZrO_2 after a cooling step from 1000 °C to room temperature (above 1000 °C plastic deformation of ZA ceramics has been observed [31], which is assumed to provide a stress-free state during cooling down to this temperature). Fig. 7(b) and (c) display histograms of the volume-weighted distribution of principal stresses for the individual phases. Compressive stresses dominate in the Al_2O_3 phase while tensile stresses are predominant in the ZrO_2 phase. The same magnitude of stresses has been observed experimentally in AZ-ceramics [32]. Usually, in the special case of ZA ceramics, the phase transition (tetragonal to monoclinic) of zirconia, which is connected with a significant volume increase of the grains must be considered. In the present study it was assumed that this phase transition was effectively suppressed by sufficient stabilization with Y_2O_3.

Rather than keeping the full data set of stresses in each finite element of the RVE, we chose to characterize any distribution of stresses by its median and the 5th and 95th percentiles. The latter can be taken as a good indicator to compare the maximum tensile stresses of different distributions, which is not prone to misinterpretations of outliers due to numerical issues.

All generated simulation data was used in the training of machine learning models to predict macroscopic material properties. For training, 75% of the data pairs were used while 25% were retained for testing. Among the regression methods available in scikit-learn, gradient boosting [33] provided the best overall results. In this method, an ensemble of weak learners (decision trees) is used to form a more capable predictor.

A separate gradient boosting model was trained for each considered material property. All models were able to predict the associated property of the microstructure with very good accuracy (cf. Table 2).

For RVEs without pores, we compare the performance of our models to some widely used analytical models for the prediction of material properties of multi-phase composites. The values predicted by each model are compared to the values of the simulated structures in the test set. The deviation of the prediction from the simulated values will be referred to as the error of the model.

The most commonly used rule-of-mixtures (ROM) considers the properties of the constituents ($P[Al_2O_3]$, $P[ZrO_2]$) and their volume fractions ($v[Al_2O_3]$, $v[ZrO_2]$) and computes an estimate by the expression

$$P[comp] = P[Al_2O_3] \cdot v[Al_2O_3] + P[ZrO_2] \cdot v[ZrO_2]$$

In addition, we consider the Hashin-Shtrikman (HS) bounds [18] which compute lower and upper bounds on the properties of a composite material. Fig. 8 displays the predicted material properties of the ROM and of our ML model when applied to the simulated RVE structures in the test set (i.e., structure-property-data that was presented to the model during training), as well as the HS bounds. The ML model gives very accurate predictions of the properties of these composites. For the two displayed material properties with approximately linear dependence on the volume fraction (elasticity, coefficient of thermal expansion) the ROM also yields reasonable estimates but shows some discrepancies, especially in the intermediate range of equally distributed volume fractions.

For other properties with a more nonlinear dependence of the material's properties on the microstructure (e.g., thermal conductivity), ROM no longer manages to give a good estimate and the HS bounds are rather conservative. Here, advanced models like Ondracek's formulas [20] allow a more accurate prediction by taking into account additional information about the microstructure. More precisely, a stereometric form factor describing the shape of the grains as well as the general structure type (inclusion vs. interpenetration) are required as an input for the Ondracek model. Fig. 9 shows the error of predictions of ROM, HS bounds, Ondracek model and the ML model, again for structures not contained in the training data set.

Both the ML model and the Ondracek model are able to predict the thermal conductivity of the composite with high accuracy, with the ML model performing slightly better. Compared to the Ondracek model, which requires rather abstract, descriptive information about the microstructure, the ML model has the added advantage of working only on easily quantifiable input parameters. In addition, it can give more diversified estimates on RVEs that differ based on their concrete microstructure but share the same volume fractions and grain shapes.

So far, we considered only nonporous composites but since samples of RVEs with porosity were contained in the training data, the ML models can also make predictions for porous structures. Fig. 10 displays the predicted Young's modulus for varying degrees of porosity. It can be observed that the prediction error is small compared to the absolute effect of the porosity on Young's modulus (cf. Fig. 5(c)).

Since the ML models can be trained on arbitrary data available from simulations, they can also make predictions for more complex quantities such as the internal stresses. Fig. 11 (a) shows the comparison of the 95th percentile of the frozen thermal tensile stresses in the ZrO_2 phase predicted by the model versus the results from the FE simulation. The ML model accurately reproduces the stresses in the structure.

The model can even be used to quantify the influence of porosity on the thermal stresses. As can be seen in Fig. 11 (b), adding pores to the structure reduces the median value of the thermal stresses in the ZrO_2 phase.

4. Conclusions

Overall, the automated numerical methodology presented in this work appears as a very flexible and reliable tool for the prediction of macroscopic material properties of ceramics composed of two or more phases in dependence of composition and microstructural parameters such as average grain size, grain size distribution or porosity. The gradient boosting ML model could be shown to enable fast and precise predictions of material properties after being trained on a few hundred

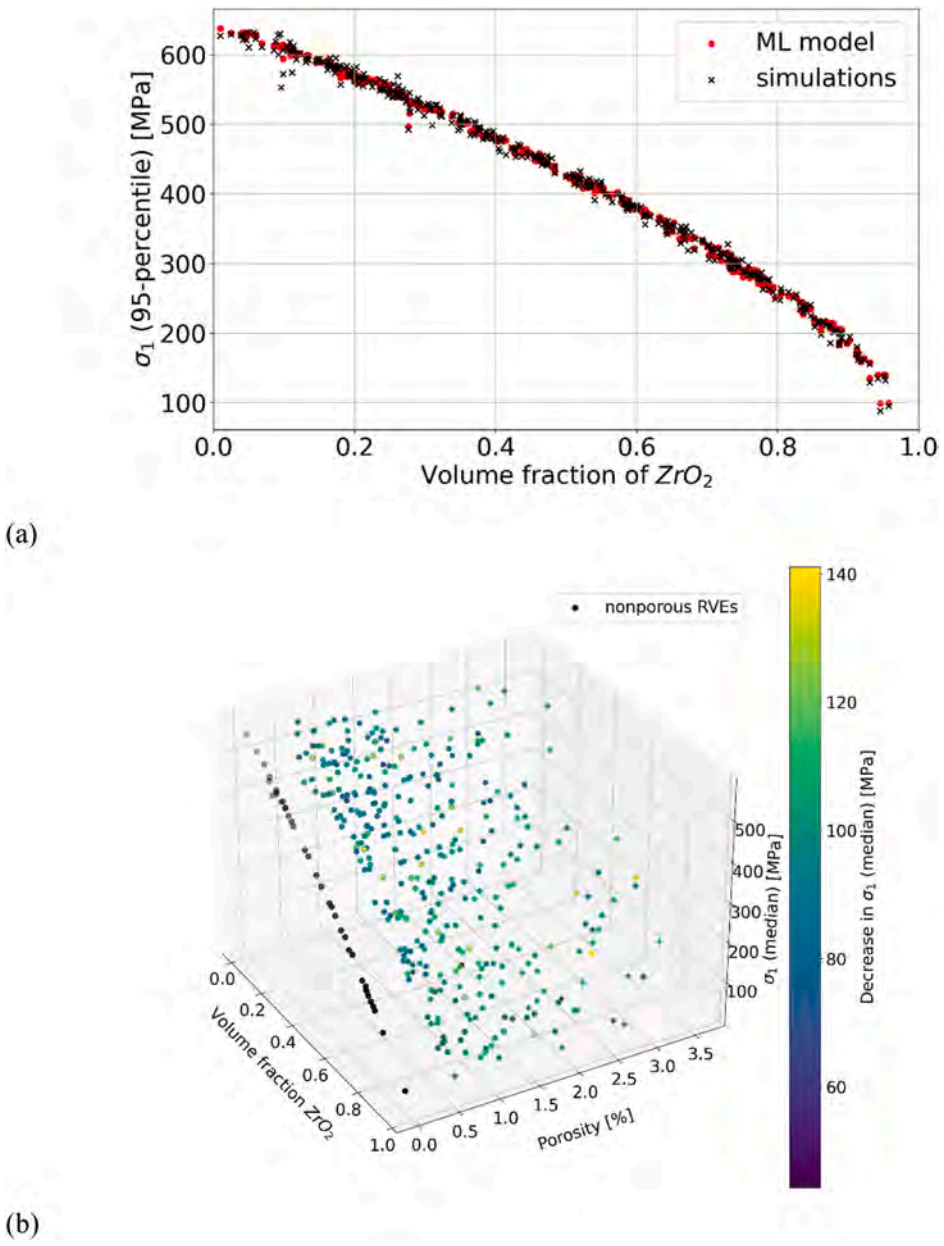

Fig. 11. (a) 95th percentile of frozen thermal stresses in the ZrO_2 phase of ZA-composites for simulated RVEs of the test set (black) and predictions of the ML model based on the structural descriptors (blue). (b) Visualization of the influence of porosity on the (median) thermal stresses in the ZrO_2 phase compared to nonporous RVEs (shown in black). (For interpretation of the references to color in this figure legend, the reader is referred to the Web version of this article.)

RVEs from a database created with an automated simulation chain. Thus, once trained the ML model can replace the time-consuming explicit simulations for the purpose of top-down design of ceramic materials, where composition and optimal microstructural parameters for a desired material behavior have to be identified. Future work has to be done to link the microstructure-property simulation to processing (e.g., sintering [34]) models. Final goal is a comprehensive digital ICME concept 'from powder to product'.

As the focus of this work was the development and test of the computational concept for fully automated microstructure-property simulation, the well-known alumina-zirconia system and several straightforward material properties (elasticity, thermal conductivity and expansion) were chosen to demonstrate and validate the capabilities of the simulation chain. While these properties could also be obtained in nearly similar quality by less complex approaches, the simulation of thermal stresses is an example for an advanced information which is highly relevant for material design, but cannot be obtained by simpler approaches. A similar situation is expected for properties like electrical impedance, where percolation phenomena or thin conductive or isolating layers in the grain boundary control the macroscopic properties in a highly nonlinear way. The described simulation chain is capable of handling such phenomena explicitly. The implementation of these aspects and their application to other ceramic composites offers a huge potential for a considerable advancement in the design of new ceramic materials.

Declaration of competing interest

The authors declare that they have no known competing financial interests or personal relationships that could have appeared to influence the work reported in this paper.

Acknowledgements

The authors wish to express their gratitude to their colleagues Marina Stepanyan and Manfred Römer for preparing the ZA samples and providing the SEM image, respectively. Financial support of this work by the Bavarian Ministry of Economic Affairs, Regional Development and Energy through the project DiMaWert is gratefully acknowledged.

References

[1] J. Allison, M. Li, M.C. Wolverton, X.M. Su, Virtual aluminum castings: an industrial application of ICME, JOM (J. Occup. Med.) 58 (2006) 28–35.
[2] A.S. Sabau, Modeling of interdendritic porosity defects in an integrated computational materials engineering approach for metal casting, Int. J. Cast Metals Res. 29 (2016) 331–337.
[3] G.J. Schmitz, U. Prahl, Integrative Computational Materials Engineering: Concepts and Applications of a Modular Simulation Platform, Wiley-VCH, Weinheim, 2012.
[4] P. Mason, Ch.R. Fisher, R. Glamm, M.V. Manue, G.J. Schmitz, A.K. Singh, A. Strachan, Proceedings of the 4th World Congress on Integrated Computational Materials Engineering (ICME 2017), Springer, 2017.
[5] S. Gajek, M. Schneider, T. Böhlke, On the micromechanics of deep material networks, J. Mech. Phys. Solid. 142 (2020), 103984.
[6] J. Kuhn, J. Spitz, P. Sonnweber-Ribic, M. Schneider, T. Böhlke, Identifying material parameters in crystal plasticity by Bayesian optimization, Optim. Eng. (2021), https://doi.org/10.1007/s11081-021-09663-7.
[7] A. Tran, T. Wildey, Solving stochastic inverse problems for property–structure linkages using data-consistent inversion and machine learning, JOM (J. Occup. Med.) 73 (1) (2021) 72–89.
[8] T. Breinlinger, A. Hashibon, T. Kraft, Simulation of the influence of surface tension on granule morphology during spray drying using a simple capillary force model, Powder Technol. (2015).
[9] T. Breinlinger, T. Kraft, Coupled discrete element and smoothed particle hydrodynamics simulations of the die filling process, Comp. Part. Mech. 3 (2016) 505–511.
[10] N. Lauro, S. Oummadi, A. Alzina, B. Nait-Ali, D.S. Smith, Computer model of drying behaviour of ceramic green bodies with particular reference to moisture content dependent properties, J. Eur. Ceram. Soc. 41 (2021) 7321–7329.
[11] A. Maximenko, O. van der Biest, Finite element modelling of binder removal from ceramic mouldings, J. Eur. Ceram. Soc. 18 (1998) 1001–1009.
[12] E.A. Olevsky, V. Tikare, T. Garino, Multi-scale study of sintering: a review, J. Am. Ceram. Soc. 89 (6) (2006) 1914–1922.
[13] F. Raether, G. Seifert, Modeling inherently homogeneous sintering processes, Adv. Theor. Simul. 1 (2018), 1800022.
[14] Y. Othmani, T. Böhlke, T. Lube, A. Fellmeth, Z. Chlup, F. Colonna, A. Hashibon, Analysis of the effective thermoelastic properties and stress fields in silicon nitride based on EBSD data, J. Eur. Ceram. Soc. 36 (2016) 1109–1125.
[15] G. Grabowski, Modelling of thermal expansion of single- and two-phase ceramic polycrystals utilising synthetic 3D microstructures, Comput. Mater. Sci. 156 (2019) 7–16.
[16] J.H. Panchal, S.R. Kalidindi, D.L. McDowell, Key computational modeling issues in integrated computational materials engineering, Comput. Aided Des. 45 (2013) 4–25.
[17] C.S. Man, M. Huang, A simple explicit formula for the Voigt-Reuss-Hill average of elastic polycrystals with arbitrary crystal and texture symmetries, J. Elasticity 105 (2011) 29–48.
[18] Z. Hashin, S. Shtrikman, A variational approach to the theory of the elastic behaviour of multiphase materials, J. Mech. Phys. Solid. 11 (1963) 127–140.
[19] J.M. Brown, Determination of Hashin–Shtrikman bounds on the isotropic effective elastic moduli of polycrystals of any symmetry, Comput. Geosci. 80 (2015) 95–99.
[20] G. Ondracek, Zur Leitfähigkeit von mehrphasigen Werkstoffen - Vergleich zwischen experimentellen und berechneten Werten von Cermets, Mater. Werkst. 5 (8) (1974) 416–428.
[21] T.M. Müller, F. Raether, 3D modelling of ceramic composites and simulation of their electrical, thermal and elastic properties, Comput. Mater. Sci. 81 (2014) 205–211.
[22] D.E.R. Winkler, T.E.M. Staab, T.M. Müller, F.G. Raether, Using a novel microstructure generator to calculate macroscopic properties of multi-phase non-oxide ceramics in comparison to experiments, Ceram. Int. 42 (2016) 325–333.
[23] D.E.R. Brockmann, T.E.M. Staab, F.G. Raether, The influence of sintering additives on the microstructure and material properties of silicon nitride ceramics investigated by advanced simulation tools, Phys. Status Solidi 214 (6) (2017), 1600634.
[24] S. Bargmann, et al., Generation of 3D representative volume elements for heterogeneous materials: a review, Prog. Mater. Sci. 96 (2018) 322–384.
[25] J. Ohser, F. Mücklich, Statistical Analysis of Microstructures in Materials Science, Wiley, 2000.
[26] B.J. Gellatly, J.L. Finney, Characterization of models of multicomponent amorphous metals – the radical alternative to the Voronoi polyhedron, J. Non-Cryst. Solids 50 (1982) 313–329.
[27] A. Kaszynski, et al., Pyansys: Python Interface to MAPDL and Associated Binary and ASCII Files, Zenodo, 2021, https://doi.org/10.5281/zenodo.5637668.
[28] T. Hastie, R. Tibshirani, J. Friedman, The Elements of Statistical Learning: Data Mining, Inference, and Prediction, second ed., Springer Series in Statistics, 2017.
[29] F. Pedregosa, et al., Scikit-learn: machine learning in Python, J. Mach. Learn. Res. 12 (2011) 2825–2830.
[30] Y. Hirata, K. Takehara, T. Shimonosono, Analyses of Young's modulus and thermal expansion coefficient of sintered porous alumina compacts, Ceram. Int. 43 (2017) 12321–12327.
[31] M. Delporte, Constrained Sintering of Zirconia, Alumina and LTCC Ceramics. PhD Thesis, Julius-Maximilians-Universität Würzburg, (Germany), 2009.
[32] K. Fan, J. Ruiz-Hervias, J. Gurauskis, C. Baudin, Residual stress measurements of alumina-zirconia ceramics by time-of-flight neutron diffraction, Mater. Res. Proc. 2 (2016) 157–162.
[33] J.H. Friedman, Greedy function approximation: a gradient boosting machine, Ann. Stat. 29 (5) (2001) 1189–1232.
[34] F. Raether, G. Seifert, H. Ziebold, Simulation of sintering across scales, Adv. Theor. Simul. 2 (2019), 1900048.